International Journal of Concrete Structures and Materials
Vol.18, No.2E, pp.79~87, September 2006

Characteristic Behavior of High-Strength Concrete Columns under Simulated Seismic Loading

Sun-Kyoung Hwang

(Received September 26, 2005, and Accepted September 9, 2006)

Abstract: The main objective of this research is to examine the behavior of high-strength concrete (HSC) columns. Eight test columns in one-third scale were tested under the conditions of cyclic lateral force and a constant axial load equal to 30% of the column axial load capacity. The 200 × 200 mm square columns were reinforced with eight D13 bars constituting a longitudinal steel ratio of 2.54% of the column cross-sectional area. The main experimental parameters were volumetric ratio of transverse reinforcement (ρ_s = 1.58, 2.25 percent), tie configuration (Type H, Type C, Type D) and tie yield strength (f_{yh} = 548.8 and 779.1 MPa). It was found that the hysteretic behaviour and ultimate deformability of HSC columns were influenced by the amount and details of transverse reinforcement in the potential plastic hinge regions. Columns of transverse reinforcement in the amount 42 percent higher than that required by seismic provisions of ACI 318-02 showed ductile behavior. At 30% of the axial load capacity, it is recommended that the yield strength of transverse reinforcement be held equal to or below 548.8 MPa. Correlations between the calculated damage index and the damage progress are proposed.

Keywords: high-strength concrete, tied columns, transverse reinforcement, seismic behavior.

1. Introduction

The response of most structures designed according to the current seismic design practice and subjected to severe earthquake is is expected to be rather inelastic. Allowing some inelastic deformations to take place and using a reduced base shear force, rather than the base shear based on elastic response, has been preferred for economic reasons. Hence, the ability of a structure to withstand a severe earthquake depends mainly on the formation of plastic hinges and its capacity to absorb and dissipate energy without a significant loss of strength. To ensure stability as well as the vertical load carrying capacity while the structure undergoes large lateral displacements, most of the building codes attempt to produce hinges in the beams rather than in the columns. However, recent earthquakes and analytical investigations[1,2] showed that the formation of plastic hinges in columns was still possible as the result of strong ground motion despite the application of "strong column-weak beam" concept, as recommended by various design codes.

Conventional methods of seismic design have the objectives of providing for life safety (strength and ductility) and damage control (serviceability drift limits). The design criteria are defined by limits on stresses and member forces calculated from prescribed levels of applied lateral shear force. In the current code-design procedures, there are uncertainties concerning the seismic demand and seismic capacity of the structure. Performance-based design[3-5] is a more general design framework in which the design criteria are expressed in terms of achieving the target performance objectives when the structure is subjected to prescribed levels of seismic hazard. The performance targets may be a level of stress not to be exceeded, a load, a displacement, a limit state or the maximum damaged state.

To establish a performance-based seismic design procedure, it is necessary to devise the evaluation methods for strength and deformation capacity of structural members with sufficient accuracy. Moreover, it is important to make it clear the relationship between the expected seismic damage, such as crack behavior and concrete crushing, and restoring force-deformation characteristics. It is required that the continuing performance of a damaged building after an earthquake can be evaluated through observed damage conditions.

Muguruma and Watanabe[6] tested eight specimens, varying the transverse reinforcement yield stress between 48 and 115 psi, while maintaining a constant volumetric ratio of 1.6%. Four tests were conducted on specimens with a strength of 12,400 psi at axial loads of 0.4 and 0.6 $f_c'A_g$. For these specimens, ultimate drifts ranged from 1.5 to 10%, showing a strong correlation between drift, axial load and the yield stress of the transverse reinforcement. The remaining four specimens had a strength of 16,800 psi and were tested at axial loads of 0.25 and 0.41 $f_c'A_g$. Ultimate drifts in this case varied between 3.0 and 8.5%. The authors concluded that high ductility could be achieved with the use of high yield transverse reinforcement.

Thompsen and Wallace[7] tested 12 specimens with a compressive strength of approximately 12,000 psi. Their cross-sectional

[1] KCI member, Dept. of Architecture, Woosong University, Daejeon 300-829, Korea. *E-mail: skhwang21@naver.com*

dimension was 6 × 6 in. Tests variables were spacing and configuration of the transverse reinforcement, yield stress of the transverse reinforcement (115 and 185 ksi) and the level of axial load (0, 0.1 and 0.2 $f_c'A_g$). Measurements indicated that the longitudinal reinforcement started to yield at a drift ratio of 1%. Strength deteriorated at drift levels beyond 2%, and severe damage occurred at drift levels higher than 4%. The longitudinal reinforcement buckled in specimens with axial loads of 0.2 $f_c'A_g$, for drift ratios greater than 4%.

Sakai and Sheikh[8] have summarized major researches conducted on the subject of confinement of concrete columns constructed using normal strength concrete (NSC). However, information on the ductility of high-strength concrete(HSC) columns has been limited,[9,10] meaning that most of the available information is based on experimental testing of small-scale columns subjected to concentric axial loads only. ACI-ASCE Committee 441[11] pointed out that columns subjected to axial loads of less than 20 percent of column axial-load capacity exhibited a good level of ductility when they are confined in accordance with current ACI confinement requirements. The scientific community has not yet reached a consensus on the required level of confinement reinforcement for ductile HSC columns.

This experimental investigation was conducted to examine the seismic performance of eight one-third scale HSC columns. The columns were subjected to a constant axial load corresponding to 30 percent of the column axial-load capacity and a cyclic horizontal load-inducing reversed bending moment. The variables studied in this research are the volumetric ratio of transverse reinforcement, tie configuration, and tie yield strength.

2. Experimental work

Eight one-third scale reinforced concrete columns were made from 68.6 MPa concrete and tested by maintaining a constant axial force ($0.3P_o$) and a cyclically applied reversed lateral load to the column. The plastic hinge region was set in the column close to the reinforced concrete foundation.

2.1 Specimens

The dimensions and steel-bar-reinforcement layout of the reinforced concrete column are shown in Fig. 1. Each specimen consisted of a 200 × 200 × 600 mm column cast integrated with a 400 × 500 × 400 mm stub. The column part of the specimen represents the parts of a regular building frame between the section of maximum moment and the point of contraflexure. The core size measured from the centre of the perimeter tie was kept constant at 174 × 174 mm for all specimens, resulting in a core area of 72 percent of the gross area of the column. Table 1 illustrates details of the test specimens. Each specimen contained eight D13 (φ = 12.7 mm) deformed bars, providing a longitudinal reinforcement ratio of 2.54 percent of the gross-sectional area of the column. Yield strength of the longitudinal steel was 430.71 MPa. The volumetric ratio of transverse reinforcement to concrete core, as measured centre-to-centre of perimeter ties, varied between 1.58 percent and 2.25 percent, and spacing of the ties varied between 27 mm and 65 mm. Type C transverse reinforcement consisted of φ6 peripheral hoops and cross ties. Type D transverse reinforcement consisted of φ6 peripheral hoops and diagonal hoops. However, Type H transverse reinforcement consisted of φ6 peripheral hoops only.

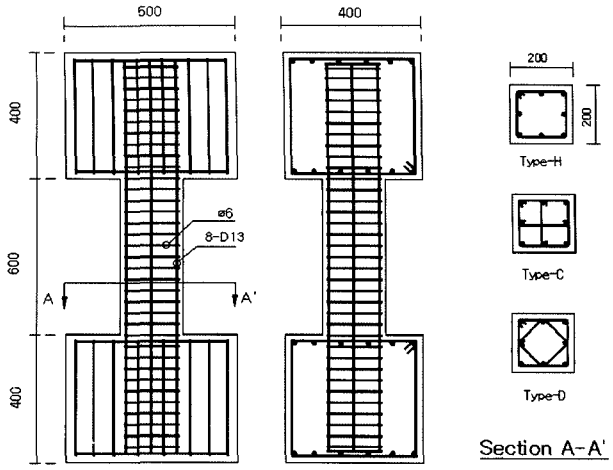

Fig. 1 Detail of specimens (unit: mm).

2.2 Materials

Ready-mix normal-weight concrete with an average slump of 210 mm was used. Forty-eight standard cylinders were cast with the specimens and were tested frequently to monitor the strength

Table 1 Properties of specimens.

Specimen	Transverse reinforcement						Longitudinal bar			f_{ck}(MPa)	Set
	Bar	s (mm)	Detail[1)]	ρ_s[2)](%)	$\rho_s/\rho_{(ACI)}$	f_{yh}(MPa)	Bar	f_y (MPa)	ρ_t(%)		
C-S	Φ6	57	C	1.58	1.00	779.10	8-D13	430.71	2.54	68.60	S-series
D-S	Φ6	65	D	1.58	1.00	779.10	8-D13	430.71	2.54	68.60	
H-S	Φ6	38	H	1.58	1.00	779.10	8-D13	430.71	2.54	68.60	
C-A	Φ6	40	C	2.25	1.42	779.10	8-D13	430.71	2.54	68.60	A-series
D-A	Φ6	46	D	2.25	1.42	779.10	8-D13	430.71	2.54	68.60	
H-A	Φ6	27	H	2.25	1.42	779.10	8-D13	430.71	2.54	68.60	
L-C-S	Φ6	40	C	2.25	1.00	548.80	8-D13	430.71	2.54	68.60	L-series
L-D-S	Φ6	46	D	2.25	1.00	548.80	8-D13	430.71	2.54	68.60	

1) Details of transverse reinforcements (C: Type C, D: Type D, H: Type H)
2) Ratio of transverse reinforcement over spacing S to core volume of concrete confined by transverse reinforcement (as measured from outside to outside)

Table 2 Concrete compressive strengths.

Average strength (MPa)					E_c (MPa)
Age (days)	7	10	21	28	33,124
Strength (MPa)	51.16	58.60	63.41	68.70	

of concrete. The 7-day strength of the concrete was about 75 percent of the 28-day concrete strength (Table 2), and, later on, the 28-day concrete strength increased by about 10 percent in the following six months. Two different types of reinforcing steel were used to construct specimens. Important properties of the steel are also listed in Table 3. The parameters f_y and f_u represent strain at the yield strength and ultimate strength, respectively; ε_y represent strain values at the onset of yield.

2.3 Instrumentation and test procedures

Several electrical strain gauges were placed in the specimens on both the longitudinal and transverse bars. The electrical strain gauges were installed in three of four sets of ties just above the stub. Curvatures were calculated from the readings of three sets of six linear variable displacement transducers (LVDTs). The LVDTs were supported by steel rods passing through the core and extending from one side of the column to the other.

The test setup and loading conditions are shown schematically in Fig. 2. Axial compression in the column was applied by a 980 kN hydraulic jack. The horizontal load was applied with a 490 kN hydraulic jack. The applied horizontal force was measured by the load cell. The horizontal tip displacement was measured by an LVDT with a range of 300 mm. The test began with the application of the axial load at the targeted value. For the first cycle of loading, the horizontal force reached 75 percent of the expected yield load. The second cycle reached the yield load, and the yield displacement was defined as the point at which longitudinal bars first yield. Thereafter, each cycle was under the displacement control with the maximum displacement being equal to 2,3,4..., times the measured yield displacement up to failure (Fig. 3). All the experimental data were stored at predetermined steps, and records were made of special occurrences such as cracking, and yielding.

Table 3. Properties of reinforcement.

	E_s (MPa)	f_y (MPa)	ε_y ($\times 10^{-6}$)	f_u (MPa)	Elongation (%)
D13	175,626	430.71	2,448	564.87	18.00
Φ6	202,860	779.10	5,700	847.70	15.20
Φ6	205,800	548.80	4,600	586.04	13.80

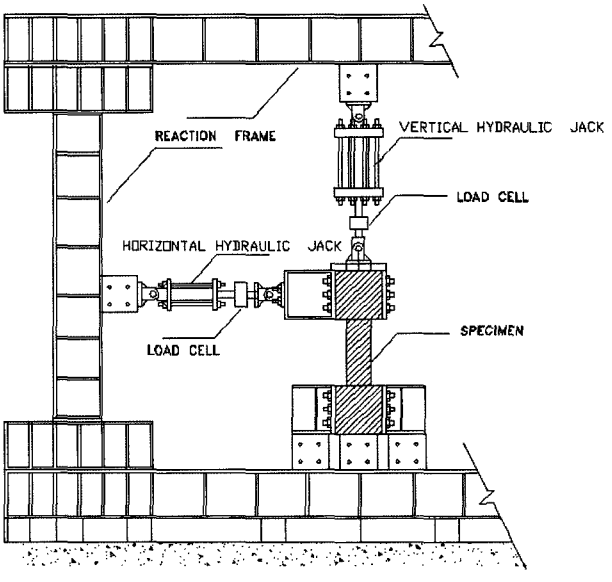

Fig. 2 Test setup and loading condition.

3. Test results

3.1 Test observations

In all specimens, the first crack occurred in the direction perpendicular to the column axis in the plastic hinge region. As lateral force increased, flexural cracking spread to 50 percent of the distance from the critical sections between the bottom end and the lateral loading point. Afterward, the longitudinal bars yielded in tension at the displacement ductility of $\mu_\Delta = 1$, and diagonal shear cracks occurred. Incipient spalling of concrete developed in the plastic hinge region at the displacement ductility of $\mu_\Delta = 2$. Spalling of cover extended as displacement increased.

In most cases, during the last cycle, buckling of the longitudinal bars was observed after yielding of the perimeter ties, which was an indication of the commencement of failure. The failure of the specimen was accompanied by extensive buckling of the longitudinal bars in all specimens. The failure mode for all specimens was mainly of flexural effects. The final appearances of all specimens are shown in Fig. 4.

3.2 Hysteretic loops

Lateral force-displacement hysteresis loops for the eight columns are shown in Fig. 4; this includes lateral force V_{if} at the ideal flexural strength based on ACI 318-02 provisions, assuming rectangular concrete stress blocks and shear force V_y at final yield of longitudinal reinforcement.

The response for the A-series specimens (Figs. 4(a),(c),(e)), which have 42 percent higher magnitude of transverse reinforcement than that required by seismic provisions of ACI 318-02, indicates better stability than for the S-series specimens up to $\mu_\Delta = 4$ or 5. This is a result of high transverse reinforcement, which enabled the transverse steel to effectively confine the core concrete, thus reducing the drastic degradation of lateral strength. The maxi-

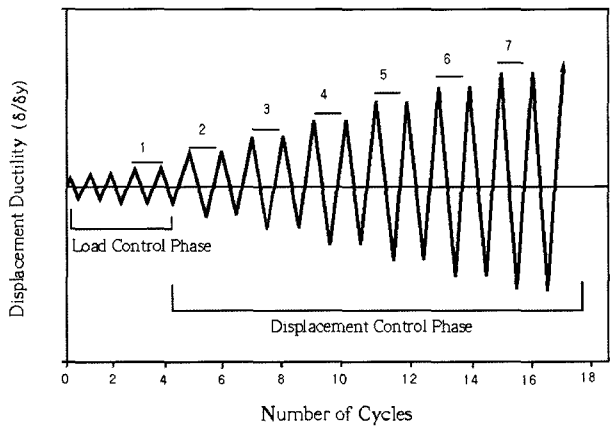

Fig. 3 Lateral displacement sequence.

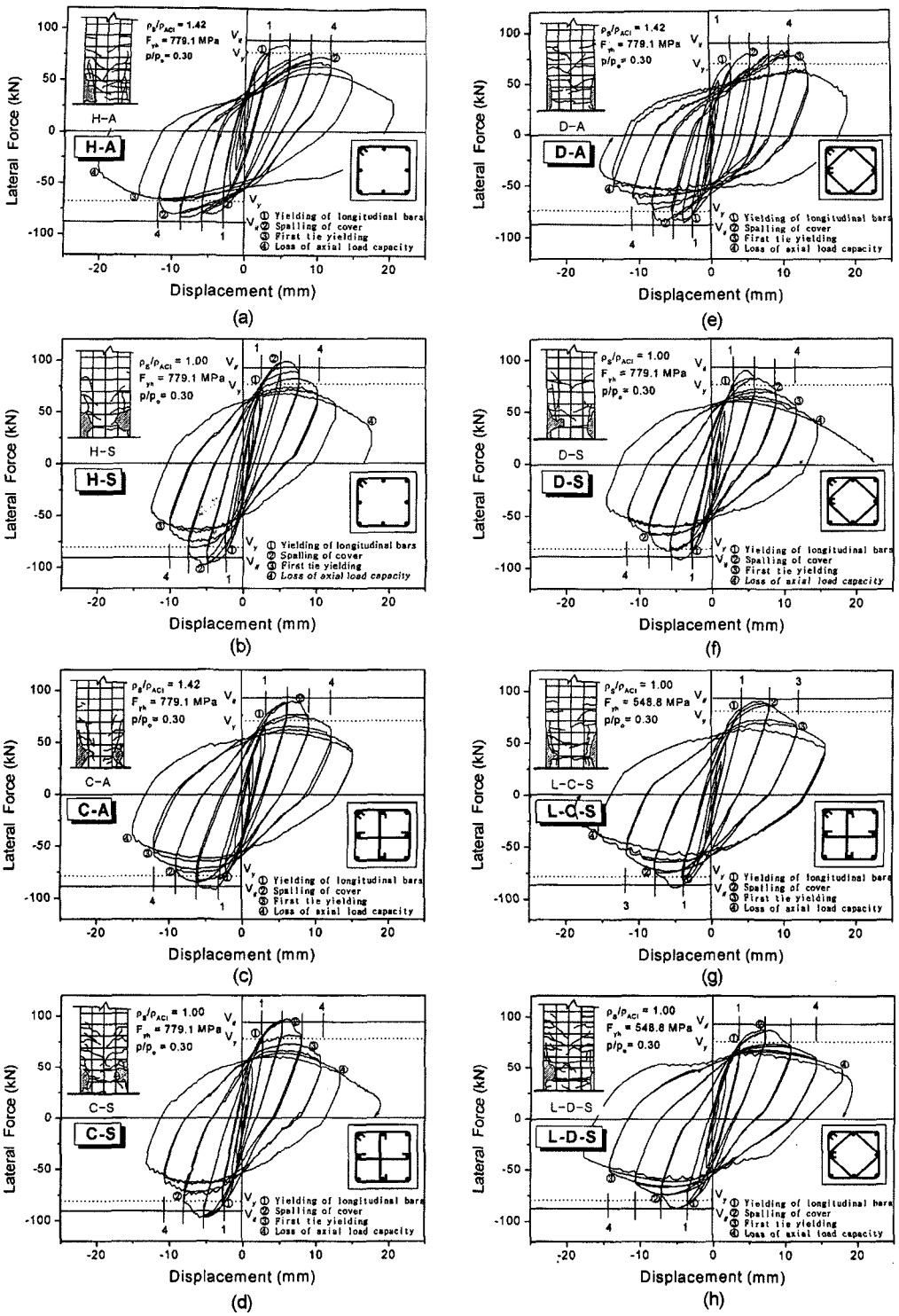

Fig. 4 Lateral load-displacement response.

mum lateral force was between 84 and 92 kN, and the index V_{max}/V_{jf} varied from 0.93 to 1.02.

The response for the S-series specimens (Figs. 4(b),(d),(f)), which have the magnitude of transverse reinforcement equal to that required seismic provisions of ACI 318-02, indicates a stable response up to μ_{Δ}= 3 or 4. Afterwards, there was a drop in lateral load-carrying capacity of the specimens at the onset of cover concrete spalling. The maximum lateral force was between 92 and 98 kN, and the index V_{max}/V_{jf} varied from 1.02 to 1.08, which exceeded the ideal lateral force as a consequence of strain hardening of longitudinal reinforcement.

The response for the L-series specimens (Figs. 4(g),(h)), having a low yield strength (548.8 MPa) of transverse reinforcement to satisfy the seismic provisions of ACI 318-02, exhibits a stable response up to μ_{Δ}= 4. The maximum lateral force was between 87 and 91 kN, and the index V_{max}/V_{jf} varied from 0.96 to 1.01.

3.3 Ductility factor and energy dissipation

It is desirable to define response indices that quantitatively describe the columns' behaviour. In seismic design, the elastic deformation is generally quantified by ductility parameters and

energy dissipation capacity. For long-period structures, it has been stated that ductility is directly related to the strength reduction factor used in most codes[11] to calculate the seismic base shear. The energy dissipation capacity is an important parameter in the design of short period structures and structures subjected to a long-duration earthquake. It also accounts for the history of loadings in addition to the maximum displacement attained. Both types of indicators are computed in this paper to compare the column behaviour on a rational basis.

Because the behaviour of reinforced concrete structures is not perfectly plastic in elasticity, it has been the general practice to define the structures' ductility parameters from a conventional diagram.[12,13] Hence, the load-displacement behaviour is idealized as a bilinear diagram, consisting of an elastic branch and an inclined post-elastic branch (Fig. 5(a)). The elastic branch is secant to the real curve at 75% of maximum horizontal load and reaches reaches the maximum horizontal load to induce the yield displacement for Δ_{yl}. The failure of the column is conventionally construed at the post-peak displacement Δ_2, where the remaining capacity of the column has dropped to 85% of the peak load. The post-elastic branch starts at point (Δ_{yl}, H_{max}) and goes to (Δ_2, H_2). H_2 is defined so that the idealized diagram and the real envelope curve have the same area under the curve, thus ensuring equal energy criteria. The sectional behaviour in terms of a moment–curvature diagram is idealized using the same procedure(Fig. 5(b)). The ductility parameters are defined from the idealized diagrams.

The ultimate displacement ductility is defined as

$$\mu_{\Delta u} = \frac{\Delta_2}{\Delta_{yl}} \tag{1}$$

and the ultimate curvature ductility is defined as

$$\mu_{\Phi u} = \frac{\Phi_2}{\Phi_{yl}} \tag{2}$$

A column is generally considered ductile if the displacement ductility ranges from 4 to 6. Table 4 provides the values of $\mu_{\Delta u}$ and $\mu_{\varphi u}$ for each column.

The energy dissipation is defined for a cycle i graphically by the hatched area in Fig. 6 or mathematically by

$$E_i = \int_A^B H' d\Delta \tag{3}$$

The total energy dissipated during the test up to 85 percent of conventional failure is

$$E_{hyst} = \sum_{i=1}^{n} E_i \tag{4}$$

where n is the number of cycles completed to reach the failure. For comparison purposes, it is convenient to normalize the dissipated energy

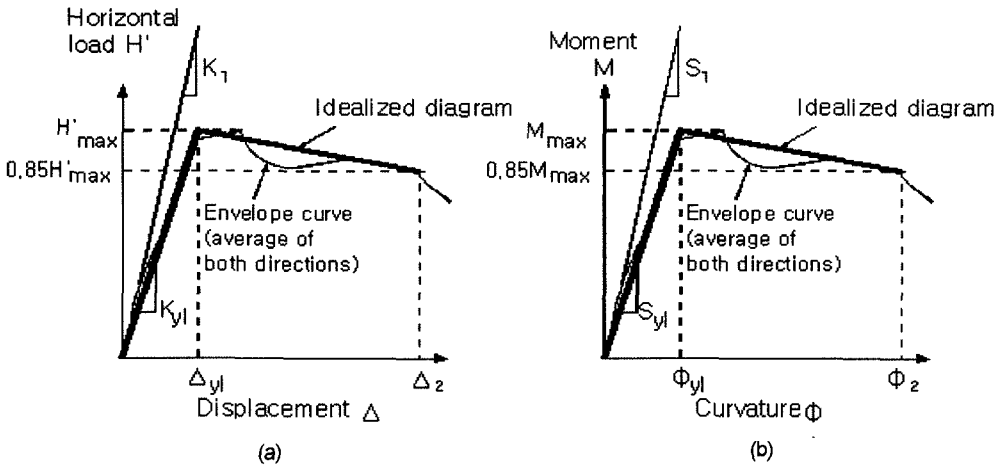

Fig. 5 Idealized curvature definitions.

Table 4. Summary of test results.

Specimen	s (mm)	Detail	ρ_s (%)	$\rho_s / \rho_{(ACI)}$	f_{yh} (MPa)	Δ_{yl} (mm)	Φ_{yl} ($\times 10^{-4}$ rad/mm)	Δ_2 (mm)	Φ_2 ($\times 10^{-4}$ rad/mm)	$\mu_{\Delta u} = \Delta_2 / \Delta_{yl}$	$\mu_{\varphi u} = \Phi_2 / \Phi_{yl}$	E_N
C-S	57	C	1.58	1.00	779	2.35	0.17	7.64	1.66	3.25	9.75	7.8
D-S	65	D	1.58	1.00	779	1.76	0.16	5.56	1.44	3.16	9.00	7.7
H-S	38	H	1.58	1.00	779	2.35	0.17	8.34	2.45	3.55	14.40	7.9
C-A	40	C	2.25	1.42	779	2.31	0.15	8.52	2.25	3.69	15.00	9.5
D-A	46	D	2.25	1.42	779	3.11	0.20	13.62	3.56	4.38	17.80	9.6
H-A	27	H	2.25	1.42	779	2.61	0.15	12.66	2.97	4.85	19.80	9.7
L-C-S	40	C	2.25	1.00	549	2.26	0.20	8.23	2.94	3.64	14.70	10.0
L-D-S	46	D	2.25	1.00	549	2.36	0.21	8.73	3.15	3.70	15.0	11.4

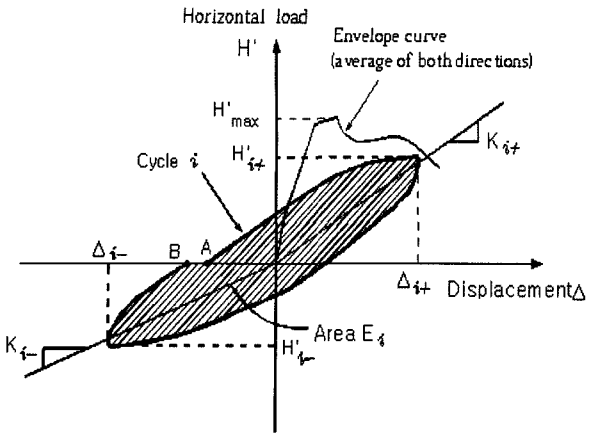

Fig. 6 Energy dissipation.

$$E_N = \frac{1}{H'_{max}\Delta_{yI}} \sum_{i=1}^{n} E_i \tag{5}$$

where, E_N is the normalized dissipated energy. To determine E_N, only cycles occurring before conventional failure are taken into account. These data are provided for each specimen in Table 4.

3.4 Strain distribution

Figs. 7 and 8 show the typical strain distribution for two test columns at different displacement-ductility ratios. The yield strain of transverse reinforcement was approximately 2,100 microstrains. As noted in Fig 7, for specimen C-A, which used higher-yield-strength steel for transverse reinforcement, the yield strain in ties was reached at relatively high displacement (11.55 mm). However, when lower-yield-strength steel for transverse reinforcement was used (see Fig. 8), yielding was observed at a low horizontal displacement of 7.91 mm.

4. Discussion of results

As mentioned previously, the effects of three variables were investigated in this experimental program; 1) the effect of steel configuration, 2) the volumetric ratio of transverse steel, and 3) the yield strength of transverse steel. It is possible to assess the effect of each variable graphically from Fig 4.

4.1 Effect of steel configuration

The effect of steel configuration on the cyclic behaviour of HSC columns can be examined by comparing the behaviour of specimens C-A, D-A, and H-A, which contain 42 percent more steel than ACI 318-02 requirements and are tested under the same level of axial load. Curvature ductility factors ($\mu_{\varphi u}$) of specimen H-A are approximately 11 and 32 percent larger than those of specimens C-A and D-A, respectively. The total energy dissipated in specimen H-A, measured by E_N, is a little larger than the energy dissipated in specimens C-A and D-A. Similar conclusions can be drawn from a comparison of the S-series, having the same amounts of transverse reinforcement required by the seismic provisions of ACI 318-02. Curvature ductility factors ($\mu_{\varphi u}$) of the specimen H-S is approximately 48 to 60 percent larger than those of specimens C-S and D-S, respectively (Table 4).

4.2 Effect of the volumetric ratio of transverse steel

The volumetric ratio of confinement steel is assessed on three

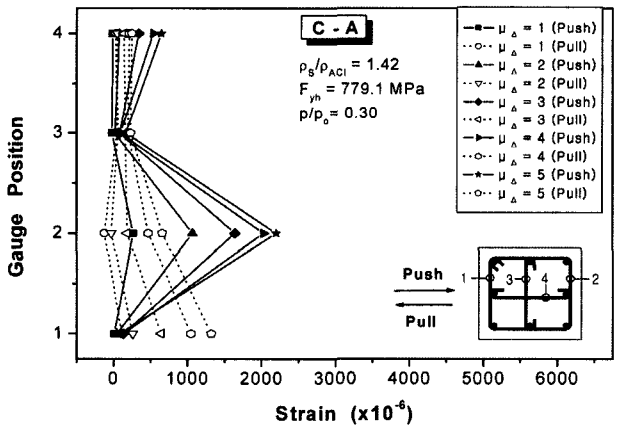

Fig. 7 Strain in transverse reinforcement at the critical region of test C-A.

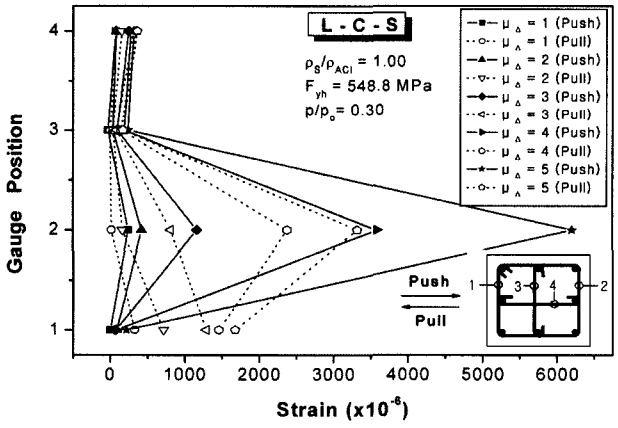

Fig. 8 Strain in transverse reinforcement in the critical region of the test L-C-S.

Table 5 Effect of the volumetric ratio of transverse steel.

Group no.	Specimen	s (mm)	Detail	ρ_s (%)	$\rho_s/\rho_{(ACI)}$	Δ_2 (mm)	Φ_2 ($\times 10^{-4}$ rad/mm)	$\mu_{\Delta u} = \Delta_2/\Delta_{yl}$	$\mu_{\varphi u} = \Phi_2/\Phi_{yl}$	E_N
1	C-S	57	C	1.58	1.00	7.64	1.66	3.25	9.75	7.8
	C-A	40	C	2.25	1.42	8.52	2.25	3.69	15.0	9.5
2	D-S	65	D	1.58	1.00	5.56	1.44	3.16	9.0	7.7
	D-A	46	D	2.25	1.42	13.62	3.56	4.38	17.8	9.6
3	H-S	38	H	1.58	1.00	8.34	2.45	3.55	14.4	7.9
	H-A	27	H	2.25	1.42	12.66	2.97	4.85	19.8	9.7

sets of columns. The first set comprises C-S and C-A. While both specimens are subjected to the same level of axial load, the volumetric ratio of the confinement steel is 1.58 percent for C-S, and 2.25 percent for C-A. Fig. 4 illustrates that specimen C-A can sustain larger inelastic cyclic displacement than specimen C-S. The results presented in Table 5 indicate that specimen C-A has a curvature ductility one and a half times that of specimen C-S. The normalized dissipated energy of specimen C-A is 22 percent higher than that of specimen C-S. The second set comprises D-S and D-A. Both specimens have the same transverse reinforcement as the experimental set of specimens C-S and C-A, respectively. Specimens in the second set, however, used detail-type D. Fig. 4 illustrates that specimen D-A can sustain larger inelastic cyclic displacement than specimen D-S. The curvature ductility of specimen D-A is about twice that of D-S, and the normalized dissipated energy of specimen D-A is 25 percent higher than that of specimen D-S. The same observations are made from an examination of the responses (Fig. 4) and the ductility parameters, as well as from the energy dissipation capacity from the third set (specimens H-S and H-A). This experimental result points to the influence of the volumetric ratio of confinement steel as an important parameter in controlling column responses.

4.3 Effect of the yield strength of transverse steel

Table 6 shows the results of four test columns that were compared to determine the effect of the yield strength of transverse reinforcement. The applied axial load for these four test columns was 30 percent of each column's axial load capacity. Results indicate that, at this axial load level, an increase in the yield strength of the transverse reinforcement had little influence on either the curvature ductility or the normalized dissipated energy E_N.

As indicated in Fig. 7, yielding of transverse reinforcement for specimen C-A was not reached until the horizontal displacement approached its maximum value. Therefore, increasing the yield strength of transversereinforcement would have no effect.

One reason for using higher strength steel for the transverse reinforcement of HSC columns is to allow larger spacing of ties. However, one should be very careful in using this approach, as it can be seen by comparing the behaviour of specimens L-C-S and C-S, in which transverse reinforcement spacing was 40 and 57 mm, respectively. Both specimens had 100 percent of the required areas for transverse reinforcement, as specified by the seismic provisions of ACI 318-02. However, the first specimen showed higher ductility. The use of higher grade steel for transverse reinforcement could satisfy ACI 318-02 requirements while having larger spacing of ties. However, at the same time, larger spacing could result in early buckling of longitudinal bars, as it was the case for the second test column.

4.4 Damage index

In recent years, a large number of damage indices have been proposed; a full review of them has been given by Williams and Sexsmith.[14] A damage index aims to give a consistent numerical indication of the damage level across a wide range of structures and loading types.

Traditional measures such as ductility and interstory drift can be useful damage indicators, but most recently proposed indices go a step further than these, by taking into account the fact that repeated loading cycles at a given amplitude generally cause greater damage than a single cycle.

The index used in this study is a modified form of the Park and Ang index, as proposed by Kunnath et al.[15] At a given cross-section, the local damage index D_L is given by

$$D_L = \frac{\phi_m - \phi_y}{\phi_u - \phi_y} + \beta_e \frac{E}{M_y \phi_u} \tag{4}$$

where, E = the cumulative energy absorbed in the hysteresis loops, β_e = the energy-related strength loss parameter, M_y = the yield moment of the section, Φ = the curvature and the subscripts m, y and u refer to the maximum value achieved, the yield value and the collapse value, respectively.

While there are some theoretical problems associated with this

Table 6 Effect of the yield strength of transverse steel.

Group no.	Specimen	s (mm)	Detail	$\rho_s / \rho_{(ACI)}$	f_{yh} (MPa)	Δ_2 (mm)	Φ_2 ($\times 10^{-4}$ rad/mm)	$\mu_{\Delta u} = \Delta_2 / \Delta_{yl}$	$\mu_{\phi u} = \Phi_2 / \Phi_{yl}$	E_N
1	C-A	40	C	1.42	779	8.52	2.25	3.69	15.0	9.5
	L-C-S	40	C	1.00	549	8.23	2.94	3.64	14.7	10.0
2	D-A	46	D	1.42	779	13.62	3.56	4.38	17.8	9.6
	L-D-S	46	D	1.00	549	8.73	3.15	3.70	15.0	11.4

Table 7 Damage progress and damage index.

Specimen	Initial crack		Spalling of cover		Shear crack		Spalling of core concrete		Crushing of core concrete	
	μ_Δ	Damage index	μ_Δ	Damage index	μ_Δ	Damage index	μ_Δ	Damage index	μ_Δ	Damage index
C-S	1	0.20	3	0.46	3	0.50	4	0.62	5	0.77
D-S	1	0.26	3	0.57	3	0.58	4	0.64	5	0.85
H-S	1	0.22	3	0.48	3	0.48	4	0.65	5	0.81
C-A	1	0.20	3	0.40	3	0.44	4	0.62	5	0.68
D-A	1	0.25	3	0.42	3	0.52	4	0.52	5	0.70
H-A	1	0.30	3	0.52	3	0.55	4	0.62	5	0.75
L-C-S	1	0.28	3	0.43	3	0.43	4	0.63	5	0.65
L-D-S	1	0.23	3	0.45	3	0.50	4	0.55	5	0.69

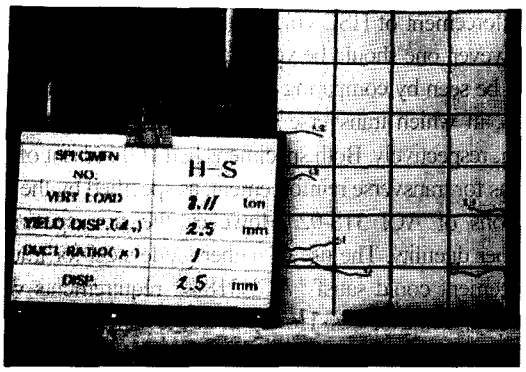

(a) at the displacement ductility ratio(μ_Δ) of 1 (Damage index = 0.22)

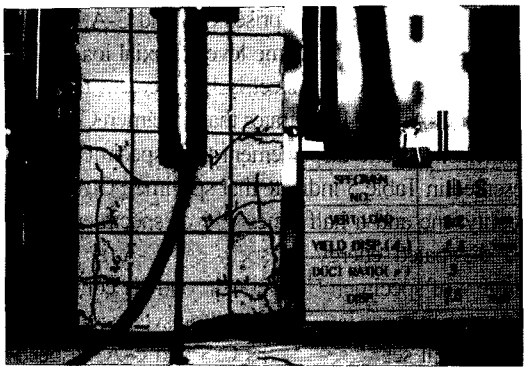

(b) at the displacement ductility ratio(μ_Δ) of 3 (Damage index = 0.48)

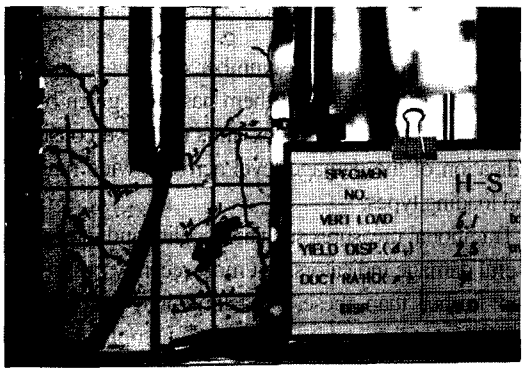

(c) at the displacement ductility ratio(μ_Δ) of 4 (Damage index = 0.65)

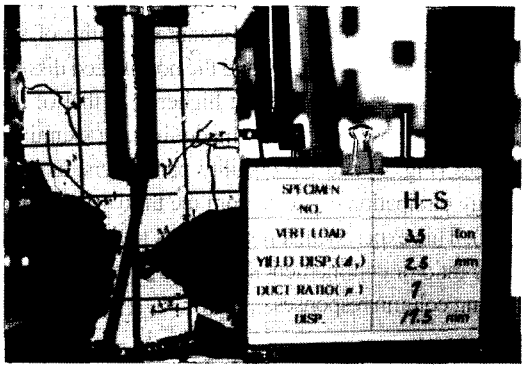

(d) at the displacement ductility ratio(μ_Δ) of 7 (Damage index = 0.86)

Fig. 9 Damage condition with respect to different damage index.

type of index, its practical advantages are numerous; (1) it is mathematically very simple; (2) it takes into accont the importance of both peak deformation and repeated cycling in the accumulation of damage; (3) it has been widely used, giving confidence in its broad applicability; and (4) several attempts have been made to come up with the correlation between the values of the index and the aforementioned damage stages.

Table 7 shows the calculated damage index and the observed damage. In most specimens, the first flexural crack occurred in the plastic hinge at the displacement ductility of $\mu_\Delta = 1$. At this point, the damage index ranged from 0.13 to 0.30.

As the amplitude of the displacement was increased, the shear cracks grew and developed into spalling of the concrete cover when the damage index was from 0.45 to 0.58. When the damage index ranged from 0.52 to 0.64, concrete crushing occurred. Afterwards, columns collapsed abruptly due to the buckling of longitudinal reinforcement when the damage index was from 0.65 to 0.85 (Fig. 9). Based on a large set (70) of previous HSC column test data[16] as well as the data from this experiment, the relationship between column performance and damage index can be summarized in Table 8 and Fig. 10.

5. Conclusions

Based on the experimental investigations discussed so far, the following conclusions are presented.

1) Specimens made of high-strength concrete with f_{ck} around 69 MPa and confined with more than 42% of the transverse reinforcement as required by the ACI 318-02 can behave in a ductile manner, showing a displacement ductility factor ($\mu_{\Delta u}$) of 4 and a curvature ductility factor ($\mu_{\Delta u}$) of over 15.

2) The use of high-strength material for transverse reinforcement (779 MPa) in HSC columns was not beneficial when axial load ratio (P/P_O) was 0.3. Therefore, for axial-load levels below 30% of the column's axial capacity, it is suggested that the yield

Table 8 Relationship between performance level and damage index.

Level	Performance level	Physical appearance	Damage index
I	Cracking	Onset of failure cracks	0. 13~0.25
II	Yielding	Theoretical first yield of longitudinal reinforcement	0.25~0.45
III	Initiation of local mechanism	Initiation of inelastic deformation Onset of concrete spalling Development of diagonal cracks	0.45~0.60
IV	Full development of local mechanism	Wide crack widths/spalling over full local mechanism region	0.60~0.75
V	Strength degradation	Buckling of main reinforcement Rupture of transverse reinforcement Crushing of core concrete	0. 75~1.00

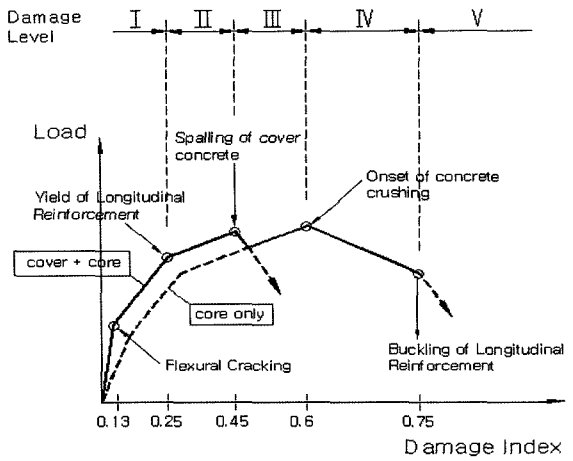

Fig. 10 Relationship between performance level and damage index.

strength of transverse reinforcement be held equal to or below 549 MPa.

3) The damage index at first flexural crack, at the time of spalling of cover concrete, and at crushing of core concrete was 0.13 to 0.30, 0.45 to 0.58, and 0.65 to 1.00, respectively.

References

1. Pauly, T., "Seismic Design of Ductile Moment Resisting Reinforced Concrete Frames, Columns: Evaluation of Actions," *Bulletin of the New Zealand National Society for earthquake Engineering*, Vol.10, No.2, June 1977. pp.85~94.

2. Bayrak, O., "High Strength Concrete Columns Subjected to Earthquake Type Loading," *M.A.Sc.* Thesis, Department of Civil Engineering, University of Toronto, Toronto, Ontario, 1995, 239pp.

3. SEAOC. Vision 2000, *Performance based seismic engineering of buildings, vols. I and II: Conceptual framework*, Sacramento(CA), Structural Engineers Association of California, 1995.

4. ATC 40, *Seismic evaluation and retrofit of existing concrete buildings*, Redwood City (CA), Applied Technology Council, 1996.

5. FEMA 273, *NEHRP guidelines for the seismic rehabilitation of buildings; FEMA 274*, Commentary, Washington(DC), Federal Emergency Management Agency, 1996.

6. Muguruma, H. and Watanabe, F., "Ductility Improvement of High Strength Concrete Columns with Lateral Confinement," *Proceedings of Second International Symposium on Utilization of High Strength Concrete, Berkeley*, May 1990, pp.20~30.

7. Thompsen, J. and Wallace, J., "Lateral Load Behavior of Reinforced Concrete Columns Constructed Using High-Strength Materials," *ACI Structural Journal*, Vol.91, No.5, September-October 1994, pp.605~615.

8. Sakai, K. and Sheikh, S. A., "What Do We Know about Confinement in Reinforced Concrete Columns?," *ACI Structural journal*, Vol.86, No.2, Mar.-Apr. 1989, pp.192~201.

9. Martinez, S., Nilson, A. H., and Slate, F. O., "Spirally Reinforced High-strength Concrete Columns," *ACI Structural journal*, Vol.81, No.5, Sep.-Oct. 1984, pp.431~442.

10. Basset, R. and Uzumeri, S. M., "Effect of Confinement on the Behavior of High-Strength Lightweight Concret Columns," *Canadian Journal of Civil Engineers*, Vol.13, 1986.

11. ACI-ASCE Committee 441, "High-Strength Concrete Columns : State of the Art," *ACI Structural Journal*, Vol.94, No.3, May-June. 1997, pp.325~335.

12. Sheikh, S. A. and Khoury, S.S., "Confined Concrete Columns with Stubs,"*ACI Structural Journal*, Vol.90, No.4, Sept.-Oct. 1993, pp.414~431.

13. Park, R., "Evaluation of Ductility of Structures and Structural Assemblages from Laboratory Testing," *Bulletin of the New Zealand National Society for Eathquake Engineering*, Vol.22, No.3, 1989, pp.155~166.

14. Williams, M. S. and Sexsmith, R. G., "Seismic damage indices for concrete structures," *A State of the Art Review*, Earthquake Spectra, Vol.11, No.2, 1995, pp.319~349.

15. Kunnath, S. K., Reinhorn, A. M., and Lobo, R. F., *IDARC 4.0: A Program for the Inelastic Damage Analysis of RC Structures, Technical Report NCEER-96-0010*, National Center for Earthquake Engineering Research, Buffalo, N. Y., 1992.

16. Lim, K. T., *A Study on Seismic Performance of High-Strength Reinforced Concrete Columns*, PhD dissertation, University of Chungnam, Korea, 1997.